

8-1-2019

# Meox2 Haploinsufficiency Accelerates Axonal Degeneration in DBA/2J Glaucoma.

Rebecca A Buchanan

Kate E Foley

*The Jackson Laboratory*, [kate.foley@jax.org](mailto:kate.foley@jax.org)

Keating W. Pepper

*The Jackson Laboratory*, [keating.pepper@jax.org](mailto:keating.pepper@jax.org)

Alaina M Reagan


*The Jackson Laboratory*, [alaina.reagan@jax.org](mailto:alaina.reagan@jax.org)

Kelly J Keezer

*The Jackson Laboratory*, [kelly.keezer@jax.org](mailto:kelly.keezer@jax.org)

*See next page for additional authors*

Follow this and additional works at: <https://mouseion.jax.org/stfb2019>

 Part of the [Life Sciences Commons](#), and the [Medicine and Health Sciences Commons](#)

---

## Recommended Citation

The authors thank Amy Bell and Mimi deVries for IOP measurements, Jeffrey Harder for training in clinical assessments, and Jennifer Ryan and In Vivo Physiology at The Jackson Laboratory for performing blood pressure measurements. They also thank Richard Libby for intellectual insights. This open access article is licensed under a Creative Commons Attribution 4.0 International License

This Article is brought to you for free and open access by the Faculty Research at The Mouseion at the JAXlibrary. It has been accepted for inclusion in Faculty Research 2019 by an authorized administrator of The Mouseion at the JAXlibrary. For more information, please contact [ann.jordan@jax.org](mailto:ann.jordan@jax.org).

---

**Authors**

Rebecca A Buchanan, Kate E Foley, Keating W. Pepper, Alaina M Reagan, Kelly J Keezer, Amanda A Hewes, Cory A Diemler, Christoph Preuss, Ileana Soto, Simon W M John, and Gareth R Howell

# *Meox2* Haploinsufficiency Accelerates Axonal Degeneration in DBA/2J Glaucoma

Rebecca A. Buchanan,<sup>1</sup> Kate E. Foley,<sup>1,2</sup> Keating W. Pepper,<sup>1</sup> Alaina M. Reagan,<sup>1</sup> Kelly J. Keezer,<sup>1</sup> Amanda A. Hewes,<sup>1</sup> Cory A. Diemler,<sup>1</sup> Christoph Preuss,<sup>1</sup> Ileana Soto,<sup>1,3,4</sup> Simon W. M. John,<sup>1,2,5,6</sup> and Gareth R. Howell<sup>1,2,6</sup>

<sup>1</sup>The Jackson Laboratory, Bar Harbor, Maine, United States

<sup>2</sup>Sackler School of Graduate Biomedical Sciences, Tufts University School of Medicine, Boston, Massachusetts, United States

<sup>3</sup>Department of Biological Sciences, Rowan University, Glassboro, New Jersey, United States

<sup>4</sup>Department of Biomedical and Translational Sciences, Rowan University, Glassboro, New Jersey, United States

<sup>5</sup>The Howard Hughes Medical Institute, Bar Harbor, Maine, United States

<sup>6</sup>Graduate School of Biomedical Sciences and Engineering, University of Maine, Orono, Maine, United States

Correspondence: Gareth R. Howell, The Jackson Laboratory, 600 Maine Street, Bar Harbor, ME 04609, USA; gareth.howell@jax.org.

Submitted: November 2, 2018

Accepted: May 20, 2019

Citation: Buchanan RA, Foley KE, Pepper KW, et al. *Meox2* haploinsufficiency accelerates axonal degeneration in DBA/2J glaucoma. *Invest Ophthalmol Vis Sci.* 2019;60:3283–3296. <https://doi.org/10.1167/iovs.18-26126>

**PURPOSE.** Glaucoma is a complex disease with major risk factors including advancing age and increased intraocular pressure (IOP). Dissecting these earliest events will likely identify new avenues for therapeutics. Previously, we performed transcriptional profiling in DBA/2J (D2) mice, a widely used mouse model relevant to glaucoma. Here, we use these data to identify and test regulators of early gene expression changes in DBA/2J glaucoma.

**METHODS.** Upstream regulator analysis (URA) in Ingenuity Pathway Analysis was performed to identify potential master regulators of differentially expressed genes. The function of one putative regulator, mesenchyme homeobox 2 (*Meox2*), was tested using a combination of genetic, biochemical, and immunofluorescence approaches.

**RESULTS.** URA identified *Meox2* as a potential regulator of early gene expression changes in the optic nerve head (ONH) of DBA/2J mice. *Meox2* haploinsufficiency did not affect the characteristic diseases of the iris or IOP elevation seen in DBA/2J mice but did cause a significant increase in the numbers of eyes with axon damage compared to controls. While young mice appeared normal, aged *Meox2* haploinsufficient DBA/2J mice showed a 44% reduction in MEOX2 protein levels. This correlated with modulation of age- and disease-specific vascular and myeloid alterations.

**CONCLUSIONS.** Our data support a model whereby *Meox2* controls IOP-dependent vascular remodeling and neuroinflammation to promote axon survival. Promoting these earliest responses prior to IOP elevation may be a viable neuroprotective strategy to delay or prevent human glaucoma.

Keywords: *Meox2*, axon degeneration, DBA/2J, myeloid cells, vasculature, gene expression

Glaucoma, the leading cause of irreversible blindness worldwide, is an amalgam of diseases that involve retinal ganglion cell (RGC) death and degeneration of the optic nerve.<sup>1,2</sup> Major risk factors include age and elevated intraocular pressure (IOP), but the molecular basis of how these factors contribute to glaucomatous damage is not well understood. In human and nonhuman primate glaucoma, increased IOP has been shown to cause changes in the optic nerve head (ONH), the area of convergence of RGC axons exiting the back of the eye.<sup>3–7</sup> These changes include increased translaminal pressure gradient, distortion of ONH biomechanical support, and excess deposition of extracellular matrix.<sup>1,8–12</sup> Determining whether these changes are primary or secondary and damaging or beneficial is challenging if one is studying human subjects alone.

Animal models are widely used to study the earliest events in a complex disease like glaucoma. Multiple models relevant to ocular hypertension (OHT) and glaucoma have shown that some of the earliest changes in the ONH involve astrocytes and microglia.<sup>13–15</sup> Among other things, these glial cells activate

immune-like processes that are likely to damage ONH structures including the neurovascular unit (NVU).<sup>16–18</sup> Previous studies have suggested the decline in blood vessel health in the optic nerve may contribute to glaucoma, and similar changes have been seen in other neurodegenerative diseases such as Alzheimer's disease, Parkinson's disease, and Huntington's disease.<sup>19,20</sup> However, which early neurovascular and glial responses are beneficial or damaging is still unclear.

Gene expression data provide a sensitive assay of molecular changes that can elucidate mechanisms of disease in tissue prior to overt morphologic changes. The ONH is an area that undergoes unique stress in OHT, and gene expression changes will prove instructive in finding the molecular mechanisms of OHT-induced glaucoma. Multiple studies, including our own, have profiled ONHs and retinas from different animal and cell models to identify genes and pathways that are modified in glaucoma.<sup>21–28</sup> These studies have used multiple models including mice, rats, primates, and human ONH astrocytes and have suggested glial-, immune-, and vascular-relevant changes in response to OHT.



In our studies, we have primarily focused on DBA/2J (D2) mice as they show asynchronous age- and IOP-dependent RGC loss that mimics hallmarks of human glaucoma.<sup>29–31</sup> Previously, microarray data of ONH and retina tissue from D2 and D2.*Gpnmb*<sup>+</sup> (a substrain of D2 that does not develop IOP elevation and RGC loss) and hierarchical clustering identified seven stages of glaucoma progression (stages 1a, 1b, 1c, 2, 3, 4, and 5) that were molecularly defined and compared to conventional morphologic analysis of axon damage in the optic nerve.<sup>27,32</sup> Stages 1a through 1c and stage 2 are considered to represent early gene expression changes that precede axon damage and other pathological signs of glaucoma.<sup>27,32</sup> Previous analyses and functional testing of this gene expression dataset have identified the activation of the complement cascade and the endothelin system as early events in D2 glaucoma.<sup>27</sup>

Here, we now reanalyze our transcriptional profiling dataset focusing on identifying key upstream regulators of the differentially expressed genes in these early molecular stages. We used upstream regulator analysis (URA) in Ingenuity Pathway Analysis (IPA) to identify putative regulators of early responses to OHT. URA identifies a cascade of upstream transcriptional regulators that can explain the observed gene expression changes in a given dataset. We identified mesenchyme homeobox 2 (*Meox2*) as a predicted regulator of multiple genes differentially expressed in early stages of D2 glaucoma. We show that *Meox2* haploinsufficiency reduces MEOX2 protein levels by approximately 44% and increases the number of eyes with axon damage compared to controls, particularly in female mice. These findings suggest that *Meox2* plays a beneficial role in response to OHT. Further, we provide data to support a model whereby vascular remodeling of the retina and myeloid cell activation in the ONH are modified by *Meox2* haploinsufficiency.

## METHODS

### Functional Analysis and Gene Set Enrichment of Differentially Expressed Genes

Data were previously generated by Howell et al.<sup>27,28,32</sup> Stage 1c genes (11,068 genes) were significantly differentially expressed (false detection rate [FDR] < 0.05) and processed through Ingenuity Pathway Analysis (IPA) (Qiagen, Inc., Redwood City, CA, USA). Fold change threshold was set at  $\pm 1.5$ . Resultant genes were processed for URA in IPA. This analysis also provided informative mechanistic networks based upon previously generated citations to create a directional map of the genes in the dataset affected by the regulator. Mechanistic network associations were available for both *Nfatc1* and *Meox2* and there were no associations for *Rcan1*, *Ikfz1*, and *Htatip2*. Mechanistic network pathway-associated genes were processed through DAVID v6.8 (Database for Annotation, Visualization and Integrated Discovery) for KEGG Pathway analysis.<sup>33</sup>

Gene ontology (GO) terms were also assessed through DAVID v6.8. The number of genes associated with each term was generated and the log of the *P* value was calculated (Benjamini corrected *P* < 0.05). Expression fold change of chosen genes was determined by the Glaucoma Discovery Platform (GDP).<sup>27,28</sup> K-means analysis was generated using genes differentially expressed (DE) across stage 2 through 5 data with basic R implementation (R Development Core Team, version 3.6.0) for six distinct clusters (k-means = 6). *Meox2* was clustered within group 3, where the associated genes were pooled for further analysis. Group 3 clustered genes were

processed for KEGG Pathway and GO term analysis as previously described (Benjamini corrected *P* < 0.05).

### Mouse Strains, Breeding, and Cohort Generation

All experiments involving mice were conducted in accordance with policies and procedures described in the Guide for the Care and Use of Laboratory Animals of the National Institutes of Health and were approved by the Institutional Animal Care and Use Committee at The Jackson Laboratory. Experiments also adhered to the ARVO Statement for the Use of Animals in Ophthalmic and Vision Research. All mice were bred and housed in a 14/10-hour light/dark cycle. All D2 mice were obtained either from The Jackson Laboratory production facility (JAX stock #000671; The Jackson Laboratory, Bar Harbor, ME, USA) or from the Howell or John Lab research colony. D2 mice are homozygous for two gene mutations, *Gpnmb*<sup>R150X</sup> and *Tyrp1*<sup>isa</sup>, and develop elevated IOP, iris stromal atrophy, and glaucoma-mediated RGC death. However, D2 mice homozygous for *Gpnmb* (*Gp*<sup>+</sup>) do not develop elevated IOP or glaucoma and exhibit only mild iris stromal atrophy. Therefore D2.*Gp*<sup>+</sup> mice (JAX stock #007048; The Jackson Laboratory) were used as a genetically matched control for D2 mice.

To create experimental strains, D2 mice were backcrossed with B6.129S4-*Meox2*<sup>CreSor</sup> (JAX stock #003755; The Jackson Laboratory) for more than six generations and then intercrossed, creating D2 mice that are heterozygous for the insertion of the cre-recombinase gene that disrupts the transcription of the *Meox2* gene, creating a *Meox2* null allele (*Mx*<sup>+/-</sup>). D2.*Gp*<sup>+</sup>*Mx*<sup>+/-</sup> were created by crossing D2.*Mx*<sup>+/-</sup> mice with D2.*Gp*<sup>+</sup> mice and then intercrossing offspring. D2 and D2.*Mx*<sup>+/-</sup> cohorts were generated by aging both males and females to 4, 8, 10.5, and 12 months with cohorts of *n* = 40 or more. D2.*Gp*<sup>+</sup> and D2.*Gp*<sup>+</sup>*Mx*<sup>+/-</sup> cohorts were generated by aging both males and females to 4 and 10.5 months with cohorts of *n* = 40 or more. Specific numbers of mice per experiment are listed with each experiment.

### Slit-Lamp Examination and IOP Measurements

D2 mice develop an iris pigment disease leading to increased OHT and resulting in axon damage and degeneration. Both males and females were evaluated for iris disease progression at 8 months using previously described methods (female D2 and D2.*Mx*<sup>+/-</sup> *n* = 30, 22, respectively; male D2 and D2.*Mx*<sup>+/-</sup> *n* = 16, 18, respectively).<sup>30</sup> IOP was measured at 8, 10.5, and 12 months of age using previously described methods (8 months: female D2 *n* = 27, D2.*Mx*<sup>+/-</sup> *n* = 39; male D2 *n* = 33, D2.*Mx*<sup>+/-</sup> *n* = 40) (10.5 months: female D2 *n* = 24, D2.*Mx*<sup>+/-</sup> *n* = 30; male D2 *n* = 20, D2.*Mx*<sup>+/-</sup> *n* = 46) (12 months: female D2 *n* = 20, D2.*Mx*<sup>+/-</sup> *n* = 22; male D2 *n* = 22, D2.*Mx*<sup>+/-</sup> *n* = 46).<sup>34,35</sup> Statistical analysis was performed using a 2-way ANOVA.

### Blood Pressure Measurements

Blood pressure was recorded using a blood pressure analysis system (BP-2000 Series II; Visitech Systems, Inc., Apex, NC, USA) as previously described with a few modifications.<sup>36</sup> Mice acclimated to the procedure room for 1 week prior to any blood pressure readings. Blood pressure was then recorded for a total of 5 days; the first 3 days of readings were used as an acclimation period and therefore no data from these days were included in analysis. The final 2 days of recordings were analyzed. Recordings were taken at the same time each day to control for circadian rhythm changes throughout the day. Additionally, the investigator was blinded to genotype while performing the readings. Each machine accommodated six

mice in restraining units and had a warming plate that maintained temperature at 38°C. Tail cuffs were placed on the base of the tail of each mouse and went through 30 rapid cycles of computer-automated inflation and deflation. Blood pressure was detected by a photoresistor cell below each tail and recorded by a computer using BP-2000 Blood Pressure Analysis software, which reported systolic and diastolic pressure and pulse. A recording was considered successful if a systolic, diastolic, and pulse reading were all reported for the cycle. For a mouse to be included in analysis, there had to be a minimum of 10 successful cycles. Then, each component of the cycle was averaged over the 2 days for each mouse. The mice tested were approximately 7 months of age and the sample sizes for each condition were as follows: D2 female, male  $n = 11, 6$ ; D2.*Mx*<sup>+/-</sup> female, male  $n = 10, 6$ . Significance between conditions was determined using a 2-way ANOVA.

### Axon Damage Assessment

Intracranial portions of optic nerves were processed and analyzed as previously described.<sup>31,37-39</sup> Optic nerves were fixed in Smith-Rudt (0.8% paraformaldehyde, 1.2% glutaraldehyde in 0.1 M phosphate buffer) for 16 hours, dissected free from the brain, processed, and embedded in plastic. One-micrometer-thick sections were then cut and stained with paraphenyldiamine (PPD). PPD darkly stains myelin sheaths and axoplasm of diseased or dying axons and lightly stains healthy axons. Two blinded investigators determined the degree of nerve damage as previously described.<sup>37,38,40,41</sup> In rare instances of a disagreement, a third investigator determined the degree of axon damage and the most common category among the three investigators was assigned. Nerves with no or early glaucoma (NOE) have no detectable glaucomatous damage and are indistinguishable from D2.*Gp*<sup>+</sup> nerves. Moderately (MOD) affected nerves have readily detectable degenerating axons (approximately 50% axon loss) as marked by darkly stained axoplasm. Severely (SEV) affected nerves have >50% axon loss and prominent gliosis. This method of assessing nerve damage has been previously validated by multiple methods including axon transport, pattern electroretinogram (PERG), axon counts, RGC soma counts, and hematoxylin and eosin staining.<sup>15,40-43</sup> Sample sizes for each experiment were as follows for females and males, respectively: 4 months D2,  $n = 47, 50$ ; 8 months D2,  $n = 65, 46$ ; 10.5 months D2,  $n = 52, 61$ ; 12 months D2,  $n = 34, 36$ ; 4 months D2.*Mx*<sup>+/-</sup>,  $n = 35, 23$ ; 8 months D2.*Mx*<sup>+/-</sup>,  $n = 58, 49$ ; 10.5 months D2.*Mx*<sup>+/-</sup>,  $n = 50, 43$ ; and 12 months D2.*Mx*<sup>+/-</sup>,  $n = 40, 61$ . To determine whether axon damage profiles were significantly different between sex, age, or genotype,  $\chi^2$  tests were performed comparing each damage level assignment per condition.

### Western Blotting of Retinas

Following ketamine/xylazine anesthesia, mice were perfused with phosphate-buffered saline (PBS) and retinas extracted. Upon removal of the eye from the animal, retinas were dissected from the globe and immediately placed on ice in 50  $\mu$ L radioimmunoprecipitation assay (RIPA) buffer. Retinal tissue was sonicated in the RIPA buffer for 10 seconds followed by 30 seconds on ice, three total intervals per tissue. Protein concentration was confirmed via Bio-Rad's DC Assay protocol (Hercules, CA, USA). Protein samples were separated by SDS-PAGE gel electrophoresis and transferred to nitrocellulose membrane. Samples were incubated with primary antibody at 4°C overnight. Prior to using horseradish peroxidase (Millipore, Temecula, CA, USA) as a secondary antibody, samples were blocked in 5% nonfat dried milk diluted in 0.1% PBS-

Tween. For detection, membranes were treated with the Amersham ECL Western blotting analysis system (GE Healthcare, Chicago, IL, USA) and imaged via chemiluminescence on Azure Biosystems (Dublin, CA, USA) cSeries Capture software. The primary antibodies used for immunoblotting were monoclonal anti-MEOX2 (predicted band size: 33.6 kilodaltons [kDa], 1:1000; Sigma-Aldrich Corp., St. Louis, MO, USA) and anti-GAPDH (glyceraldehyde 3-phosphate dehydrogenase) (predicted band size: 35.8 kDa, 1:1000; Abcam, Cambridge, MA, USA). Blots were stripped after MEOX2 assessment and prior to GAPDH assessment (loading control) using standard procedures.

### Immunofluorescence of Optic Nerve Heads

Female mice were killed by cervical dislocation, their eyes enucleated and placed in 4% paraformaldehyde (PFA) overnight. Following fixation, eyes were placed in a 30% glucose gradient and frozen in optimal cutting temperature (OCT) compound, and ONHs were cryosectioned at 10- $\mu$ m thickness.

For immunostaining against vascular-associated proteins, one section per eye was used to constitute cohorts: 4 months D2,  $n = 6$ ; 8 months D2,  $n = 4$ ; 10.5 months D2,  $n = 6$ ; 4 months D2.*Mx*<sup>+/-</sup>,  $n = 6$ ; 8 months D2.*Mx*<sup>+/-</sup>,  $n = 4$ ; 10.5 months D2.*Mx*<sup>+/-</sup>,  $n = 4$ ; 4 months D2.*Gp*<sup>+</sup>,  $n = 3$ ; 10.5 months D2.*Gp*<sup>+</sup>,  $n = 6$ ; 4 months D2.*Gp*<sup>+</sup>*Mx*<sup>+/-</sup>,  $n = 6$ ; 10.5 months D2.*Gp*<sup>+</sup>*Mx*<sup>+/-</sup>,  $n = 6$ . ONH sections were brought to room temperature (RT), pretreated with H<sub>2</sub>O at 37°C for 3 minutes, then treated with 0.5 mg/mL pepsin (Sigma-Aldrich Corp.) in 0.2 N HCl at 37°C for 10 minutes. Sections were then washed twice with 1 $\times$  PBS for 10 minutes at RT and then incubated with primary antibody (rabbit anti-laminin [1:300] L9393; Sigma-Aldrich Corp.) and goat anti-CD31 [1:40]; MAB3628; R&D Biosystems, Minneapolis, MN, USA) diluted with 10% normal donkey serum in PBT (1 $\times$  PBS + 1% Triton X-100) overnight at 4°C. Sections were then washed three times with PBT for 10 minutes at RT and then incubated with secondary antibody (donkey anti-rabbit AF488 [1:800]; A-21206; ThermoFisher Scientific [Waltham, MA, USA] or donkey anti-goat AF594 [1:800]; A-11058; ThermoFisher Scientific) diluted in PBT at RT for 4 hours. Following secondary incubation, sections were washed three times with 1 $\times$  PBS for 10 minutes at RT, incubated with 4',6-diamidino-2-phenylindole (DAPI) (1:1000) diluted in 1 $\times$  PBS for 20 minutes, then washed once with 1 $\times$  PBS for 5 minutes at RT. Following immunostaining, slides were mounted with Aqua Poly-Mount (Polysciences, Warrington, PA, USA).

For immunostaining against non-vascular-associated proteins, one section per eye was used to constitute cohorts: 4 months DBA/2J,  $n = 5$ , 8 months DBA/2J,  $n = 10$ , 10.5 months DBA/2J,  $n = 6$ ; 4 months D2.*Mx*<sup>+/-</sup>,  $n = 7$ ; 8 months D2.*Mx*<sup>+/-</sup>,  $n = 11$ ; 10.5 months D2.*Mx*<sup>+/-</sup>,  $n = 4$ ; 4 months D2.*Gp*<sup>+</sup>,  $n = 3$ ; 10.5 months D2.*Gp*<sup>+</sup>,  $n = 6$ ; 4 months D2.*Gp*<sup>+</sup>*Mx*<sup>+/-</sup>,  $n = 6$ ; 10.5 months D2.*Gp*<sup>+</sup>*Mx*<sup>+/-</sup>,  $n = 7$ . ONH sections were brought to RT, washed once with PBT for 15 minutes, and then incubated with primary antibody (goat anti-IBA1 [1:200]; ab5076; Abcam) in 10% normal donkey serum in PBT ON at 4°C. The secondary antibody and remaining steps were the same as for vascular-related proteins listed above.

Images of immunofluorescence (IF) assays were obtained with consistent exposure times per channel across all samples. The exposure time for each sample was determined by taking 20 blinded samples, finding the best exposure by the "auto-exposure" function in the ZEN Pro program (ZEISS, Munich, Germany), and finding the median exposure time per channel between the 20 blinded samples. For myeloid cell number quantification, the area considered to be the ONH was the area from the sclera and down 200  $\mu$ m and to the outer margins.



This area was measured, drawn, and calculated using ImageJ (National Institutes of Health, Bethesda, MD, USA). Once the area was determined, colocalization of DAPI and IBA1 staining indicated a positive myeloid cell. Cell number was calculated and reported as a cell number per area. Significance between cohorts was determined by 2-way ANOVA.

### Immunofluorescence of Whole Retinas

Following ketamine/xylazine anesthesia, mice were perfused with PBS. Eyes were enucleated and immersion fixed in 4% paraformaldehyde and processed as previously described.<sup>44</sup> Briefly, eyes were hemisected and retinas dissected under a stereomicroscope (Nikon SMZ800, Tokyo, Japan), permeabilized with 1% Triton X-100 in PBS, blocked with 10% normal donkey serum in 0.1% Triton X-100 in PBS, and incubated with the following primary antibodies at 4°C overnight: goat anti-type IV collagen (1:40; EMD Millipore, Darmstadt, Germany) and rabbit anti-Iba1(1:200; Wako Chemicals USA, Richmond, VA, USA).

After washing with 0.1% Triton X-100 in PBS (3 × 15 minutes), retinas were incubated with the appropriate fluorophore-conjugated secondary antibodies (1:500; Life Technologies, Carlsbad, CA, USA) at 4°C overnight. After another washing with 0.1% Triton X-100 in PBS, four or five radial cuts were made in the retinas, from the edge toward the ONH, ganglion cell layer up, for flat mounting in Aqua-Poly/Mount (Polysciences). Imaging was performed using the TCS SP8 confocal laser scanning microscope (Leica, Wetzlar, Germany), and then processed with ImageJ. All images were taken from the peripheral retina, and the total vascular area per image was assessed using AngioTool software.<sup>45</sup> Using standard parameters described by AngioTool, the area covered by a vascular network was calculated for each image.<sup>45</sup> Four images from each retina were assessed within a cohort, and statistics were generated by averaging all areas/eye for  $n = 1$ .

## RESULTS

### Meox2 Is Predicted to Be an Upstream Regulator of Responses to Ocular Hypertension

To identify putative regulators of early gene expression changes, URA was performed on genes DE (FDR < 0.05, fold change > +1.5 or < -1.5) in stage 1c (Supplementary Table S1). The top five transcription factors were *Hiatip2*, *Nfatc1*, *Rcan1*, *Meox2*, and *Irfz1* (Fig. 1A). These transcription factors are predicted to directly regulate between 34 and 6 genes in stage 1c (Fig. 1B; Supplementary Table S2). Expression of these transcription factors steadily increased from stage 1a to stage 1c, suggesting their upregulation may have downstream effects on multiple target genes and disease progression (Fig. 1C). Only two of the top five transcription factors (*Nfatc1* and *Meox2*) were predicted by IPA to have associated mechanistic networks (i.e., networks of genes that are predicted by the URA to explain patterns in the gene expression data). The *Nfatc1* network contained 653 genes (Supplementary Table S3) while the *Meox2* network contained 364 genes (Fig. 1D; Supplementary Table S4). The *Nfatc1* and *Meox2* mechanistic networks showed overlapping enriched KEGG pathways including cytokine–cytokine receptor interaction, PI3K-AKT signaling pathway, osteoclast differentiation, phagosome, focal adhesion, and ECM–receptor interactions (Figs. 1E, 1F), which suggested a possible role for both genes in regulating inflammatory and vascular responses. Given the similarity of the predicted functions of the *Nfatc1* and *Meox2* mechanistic networks, previous work on *Nfatc1* and related genes such as

calcineurin in RGC degeneration, and the novelty of the predicted role for *Meox2* in glaucoma, we chose to prioritize *Meox2* for further study.<sup>46–50</sup>

*Meox2* first becomes significantly upregulated in stage 1c (Fig. 1C). Therefore, to further investigate the role of *Meox2*, we identified the GO terms enriched in stage 1c that were assigned to *Meox2*. Three enriched GO terms met this criterion: “angiogenesis,” “positive regulation of transcription from RNA pol II promoter,” and “transcription DNA-templated” ( $P = 1.37 \times 10^{-7}$ ,  $P = 8.97 \times 10^{-7}$ , and  $P = 4.26 \times 10^{-5}$ , respectively) (Fig. 2A). Angiogenesis, the most significant term, is a GO term associated at multiple molecular stages of glaucoma (Fig. 2B). Angiogenesis genes upregulated in stage 1c show a comparable gene expression profile across the molecular stages of disease to *Meox2* (Fig. 2C).

To further understand possible mechanism(s) by which *Meox2* contributes to D2 glaucoma, k-means clustering was performed to identify genes that respond similarly across the molecular stages of disease. K-means clustering ( $k = 6$ ) was performed on a set of 4137 genes that were DE across stages 2 through 5. We selected these genes because *Meox2* is first DE in stage 1c (Fig. 1) and so we hypothesized that the downstream responders to *Meox2* would be present in stages 2 through 5. Five clusters of genes were identified (group 6 is considered an unclustered group, Fig. 3A). *Meox2* clustered with genes in group 3. Genes within group 3 were then examined by KEGG Pathway analysis. *Meox2* is not yet associated with a KEGG pathway, but genes within group 3 were enriched for lysosome, phagosome, other glycan degradation, and osteoclast differentiation (Fig. 3B). These pathways are associated with inflammation and myeloid cell activity. In support of this, GO term enrichment showed that group 3 genes were enriched for extracellular exosome, lysosome, and external side of plasma membrane (Fig. 3C). These GO terms were similar to those identified by IPA in the *Meox2* mechanistic network (Fig. 1F). Genes in these enriched KEGG pathways that also had myeloid-related GO terms included *Trem2*, *Tyrobp*, and *Itgax* (*Cd11c*) and, as predicted by the k-means analyses, showed a similar pattern of gene expression across the molecular stages of disease as *Meox2* (Fig. 3D). Additionally, the genes within the GO term “extracellular exosome” included basement membrane and transport genes such as *Itgb2*, *Itgb3*, *Timp2*, and *Ctsz* (Fig. 3E).

Collectively, our data suggest that *Meox2* is mediating early processes in the ONH involving interactions between myeloid cells (that may involve resident microglia, monocytes, and/or macrophages) and neurovascular-related cells.

### Meox2 Haploinsufficiency Does Not Cause Overt Changes to Vasculature or Myeloid Cells in ONH or Retina of Young DBA/2J Mice

Mice deficient in *Meox2* (*Meox2*<sup>-/-</sup>) are embryonic lethal due to a variety of phenotypes including abnormal vascular development; however, previous studies by us and others have shown that *Meox2* haploinsufficiency can modify phenotypes in other neurodegenerative disease models.<sup>51,52</sup> Given its role in development, we assessed ONHs and retinas in young *Meox2* haploinsufficient D2s and controls. We first performed a Western blot on the retinas of young D2 and D2.*Mx*<sup>+/-</sup> mice to assess MEOX2 protein levels. No significant differences in MEOX2 protein levels were detected comparing D2 and D2.*Mx*<sup>+/-</sup> mice (Fig. 4A). Given that *Meox2* is associated with vascular remodeling including angiogenesis, we then sought to determine if there were any differences in the vasculature and surrounding basement membrane in the ONH and retinas of young D2.*Mx*<sup>+/-</sup> mice. No observable

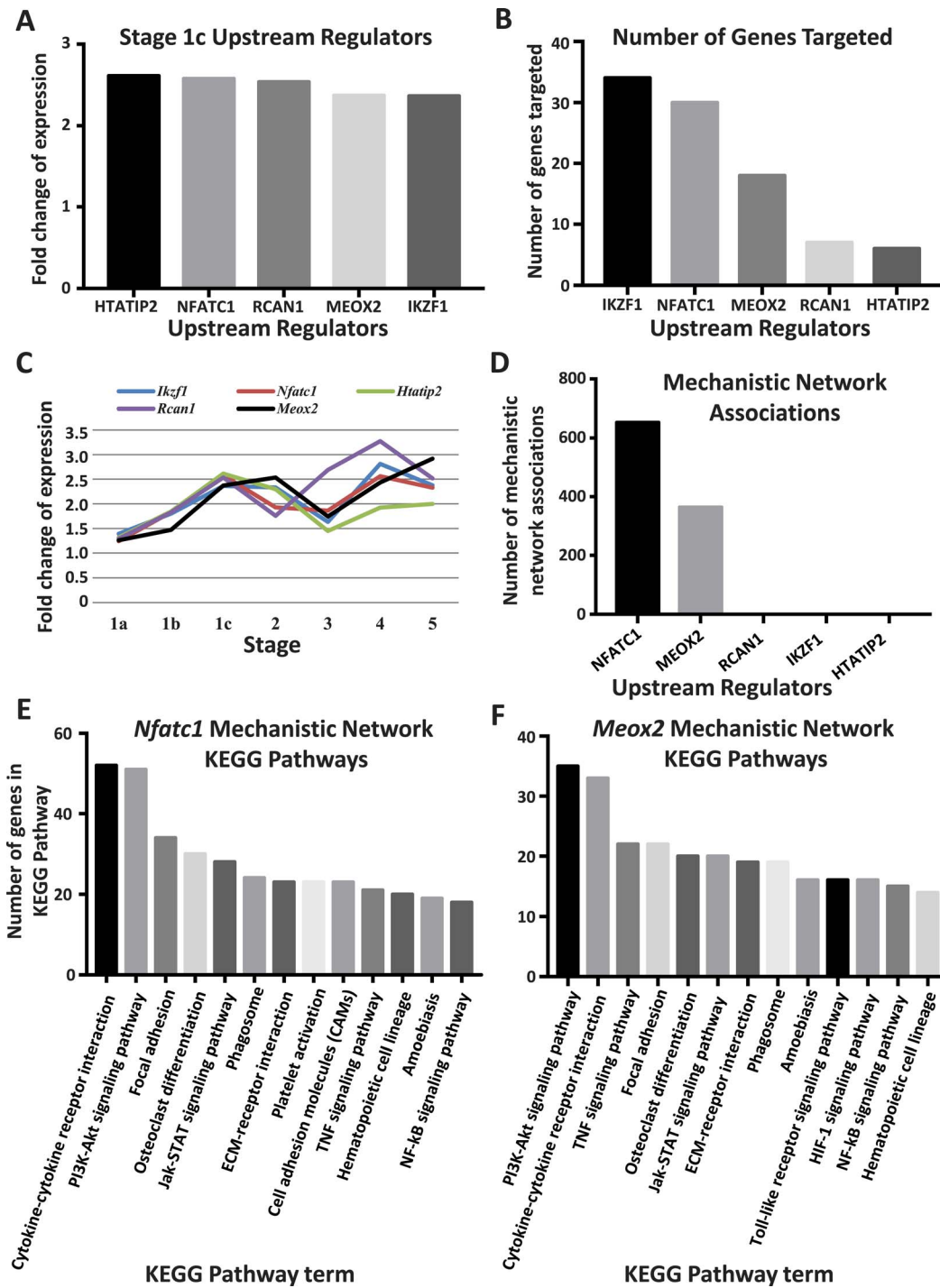


**FIGURE 1.** *Meox2* is an early upstream regulator of genes that have significant fold changes of expression early in D2 glaucoma. (A) Upstream regulator analysis on DE genes (FDR < 0.05) from stage 1c with a fold change greater than |1.5| was performed. This analysis determined *Htatip2* (FC = 2.612,  $P = 3.65 \times 10^{-2}$ ), *Nfatc1* (FC = 2.577,  $P = 1.80 \times 10^{-1}$ ), *Rcan1* (FC = 2.537,  $P = 1.19 \times 10^{-1}$ ), *Meox2* (FC = 2.373,  $P = 1.76 \times 10^{-6}$ ), and *Ikzf1* (FC = 2.365,  $P = 1.08 \times 10^{-2}$ ) to be the top five regulatory transcription factors (TFs) at this stage. (B) Each of the top five regulatory TFs was further analyzed to determine the predicted number of genes targeted. (34, 30, 18, 7, and 6 genes targeted, respectively). (C) To understand the expression behavior of the top five regulatory TFs through the stages of D2 glaucoma, the fold change of expression over the seven stages was analyzed. Each of the five TFs had a similar expression pattern; all but *Meox2* first becomes significant at stage 1b (*Meox2* at stage 1c), remaining upregulated through stage 5. (D) Next, the number of mechanistic network associations for each TF was found. *Nfatc1* and *Meox2* were the only upstream regulators that were associated with mechanistic networks (653 and 364 genes, respectively). (E) KEGG Pathway analysis of genes in the *Nfatc1* mechanistic network associations found pathways associated with inflammation, cell-cell interactions, and basement membrane turnover (FDR < 0.05). (F) KEGG Pathway analysis of genes in the *Meox2* mechanistic network associations found pathways associated with inflammation, cell-cell interactions, and basement membrane turnover (FDR < 0.05).

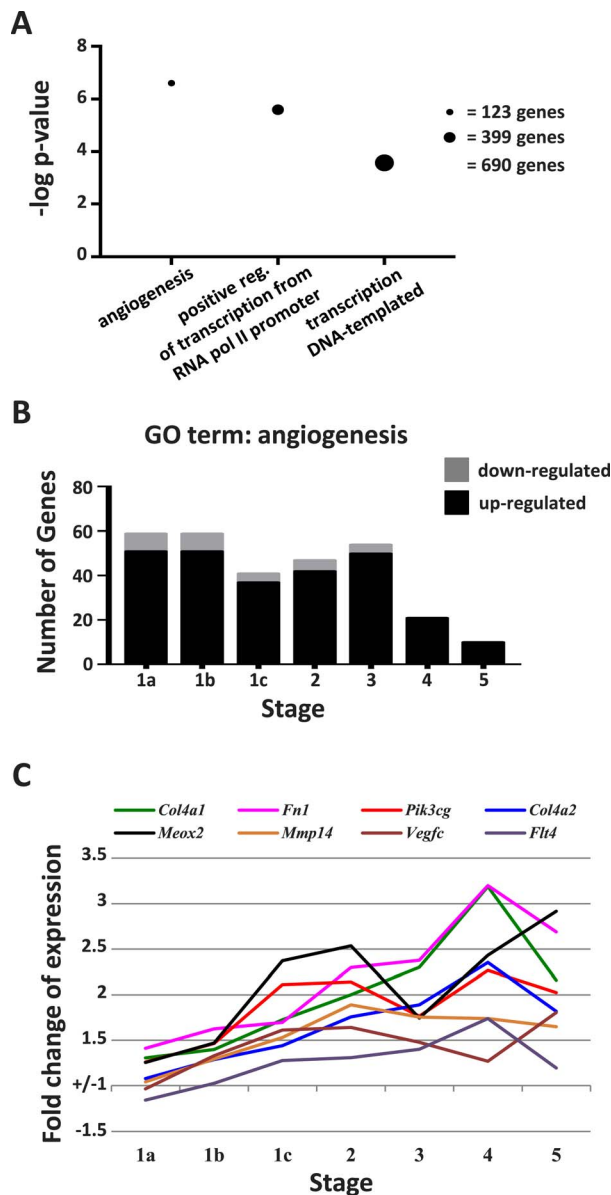


**FIGURE 2.** Gene ontology (GO) enrichment analysis of microarray data of D2 glaucoma identifies *Meox2* in GO terms associated with angiogenesis. (A) Gene ontology enrichment analysis of microarray data obtained by comparing D2 and D2.*Gp*<sup>+</sup> controls found the  $-\log(P)$  value of the three most significant GO terms by Benjamini corrected  $P < 0.05$  were “angiogenesis” ( $P = 1.35 \times 10^{-7}$ ), “positive regulation of transcription from RNA pol II promoter” ( $P = 8.97 \times 10^{-7}$ ), and “transcription DNA-templated” ( $P = 4.26 \times 10^{-5}$ ). The size of the circle associated with the GO term corresponds with the number of genes within that term (angiogenesis = 123 genes, positive regulation of transcription from RNA polymerase II promoter = 399 genes, transcription DNA-templated = 690 genes). (B) The number of differently expressed genes in the GO term “angiogenesis” at each molecularly defined stage of glaucoma that are either up- or downregulated at that stage. (C) Fold change of expression at each molecularly defined state of glaucoma of a selection of genes from the GO term “angiogenesis” and *Meox2* was graphed. These genes are related to basement membrane (*Col4a1*, *Col4a2*), blood clotting (*Fn1*), cell proliferation (*Pik3cg*), breakdown of extracellular matrix (*Mmp14*), and receptor for vascular endothelial growth factors (*Flt4*). *Col4a1*, *Fn1*, and *Pik3cg* all become significantly upregulated at stage 1b and continue through stage 5; *Col4a2*, *Meox2*, and *Mmp14* all become significantly upregulated at stage 1c and continue through stage 5; *Vegfc* and *Flt4* become significantly upregulated in stage 1c; *Vegfc* remains significant except for stage 4; *Flt4* remains significant through stage 4.

differences were identified in CD31, an endothelial cell marker, and laminin, a basement membrane marker, in ONHs (Figs. 4B, 4C). Further, no significant differences were seen in retinal vascular area comparing D2 and D2.*Mx*<sup>+/-</sup> mice (Fig. 4D). Analysis of *Meox2* also suggested a role in myeloid cell function and neuroinflammation (Figs. 1–3); therefore we stained for IBA1 (a marker of myeloid cells including resident microglia, monocytes, and macrophages) in both the retina and ONH and counted the number of positively stained cells. Again, we found no significant differences in IBA1+ myeloid cell numbers in the retina (Fig. 4E) or in the ONH (Figs. 4F, 4G) comparing D2 and D2.*Mx*<sup>+/-</sup> mice. It is also of note that the morphology of the myeloid cells was consistent with being in the sensing (ramified) rather than the activated amoeboid state.

### *Meox2* Haploinsufficiency Increases the Numbers of DBA/2J Eyes With Axon Damage

Upon finding no overt differences in vessel coverage or myeloid cell number and morphology at a young age, we functionally tested the effect of *Meox2* haploinsufficiency in D2 glaucoma. Cohorts of D2, D2.*Mx*<sup>+/-</sup>, D2.*Gpnmb*<sup>+</sup> (D2.*Gp*<sup>+</sup>), and D2.*Gp*<sup>+</sup>*Mx*<sup>+/-</sup> mice were established. D2 mice develop an iris pigment disease resulting in OHT-dependent RGC death. In our D2 colonies, the iris disease (iris pigment dispersion and iris stromal atrophy) is evident at 6 months of age with OHT apparent in significant numbers of eyes between 8 and 10 months. RGC loss occurs in few eyes at 9 months or younger and many eyes between 10 and 12 months. Therefore, cohorts were generated to track glaucoma-relevant phenotypes at 8, 10.5, and 12 months. Axon damage was also assessed in cohorts of young (4 months) mice.

To determine whether *Meox2* haploinsufficiency affected the normal progression of iris disease, slit-lamp examinations were performed on eyes from mice of all genotypes at approximately 8 months (Fig. 5A). Clinical assessment found no significant differences between eyes from D2 and D2.*Mx*<sup>+/-</sup> mice, suggesting that *Meox2* haploinsufficiency did not affect the normal progression of the D2 iris disease. Additionally, D2.*Mx*<sup>+/-</sup> mice showed a similar age-dependent increase in IOP as D2 mice. There were no statistically significant differences in IOP profiles comparing different genotypes within age and sex (Fig. 5B). Furthermore, given the previously reported role for *Meox2* in vascular development and maintenance, and the association between blood pressure and glaucoma risk,<sup>53–55</sup> blood pressure was determined in D2 and D2.*Mx*<sup>+/-</sup> mice. *Meox2* haploinsufficiency did not affect blood pressure in either females or males when compared to wild-type controls (Fig. 5C).

We next analyzed the degree of axon damage using PPD staining of cross sections of optic nerves from all mice of all cohorts. Each eye was assigned to one of three categories: no axon damage, moderate axon damage, and severe axon damage (Fig. 6A). This method of axon damage assessment allows us to detect small but significant changes due to our ability to include large numbers of optic nerves in the analysis, which is necessary since D2 glaucoma is complex and asynchronous. No eyes from young (4 months) mice of any genotype showed any axon damage, indicating that *Meox2* haploinsufficiency is not sufficient to induce axon damage due to developmental effects (Fig. 6B). At 8 months, approximately 13% of D2 males had damage compared to 8% of D2.*Mx*<sup>+/-</sup> males, and 11% of D2 females compared to 36% of D2.*Mx*<sup>+/-</sup> females ( $P = 0.443$  and  $P = 4.58 \times 10^{-9}$  respectively). At 10.5 months, approximately 67% of D2 males had axon damage compared to 77% of D2.*Mx*<sup>+/-</sup> males, and 64% of D2 females compared to 90% of D2.*Mx*<sup>+/-</sup> females ( $P = 0.00835$  and  $P = 0.000558$ , respectively). At 12 months, approximately 61% of D2 males had damage compared to 67% of D2.*Mx*<sup>+/-</sup> males, and 82% of D2 females



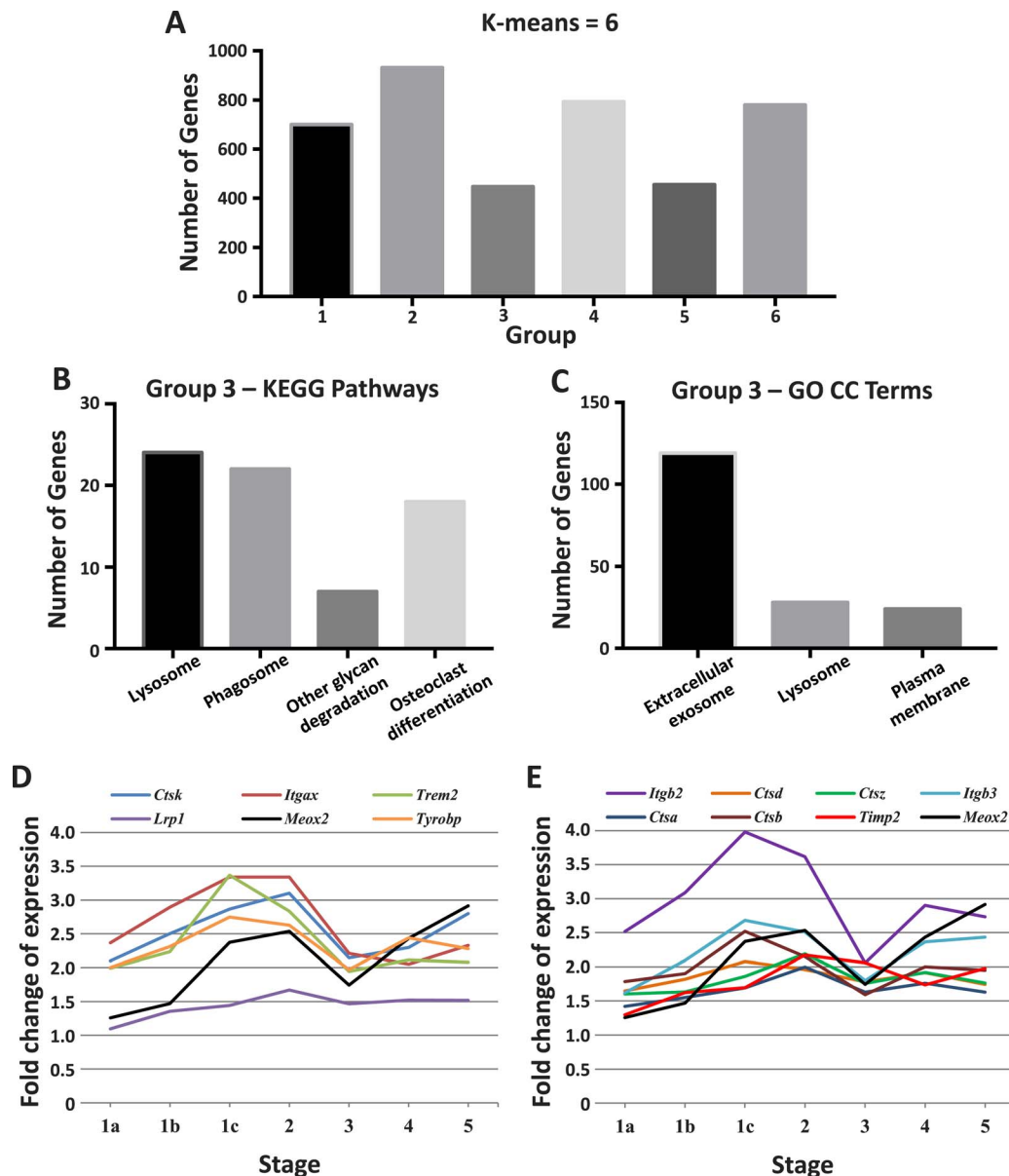


**FIGURE 3.** K-means analysis identifies *Meox2* clustered with genes enriched for inflammatory pathways. (A) K-means clustering ( $k = 6$ ) of genes differentially expressed through stages 2 through 5 identified five groups of genes with similar gene expression patterns across the stages (number of genes: group 1 = 700, group 2 = 931, group 3 = 477, group 4 = 794, group 5 = 455, and group 6 = 780). *Meox2* is in group 3. Group 6 contains unclustered genes. (B) KEGG Pathway analysis on *Meox2*-containing group 3 reported “lysosome,” “phagosome,” “other glycan degradation,” and “osteoclast differentiation” as the most significant pathways by Benjamini corrected  $P < 0.05$  ( $P = 9.69 \times 10^{-9}$ ,  $P = 4.24 \times 10^{-5}$ ,  $P = 2.21 \times 10^{-4}$ , and  $P = 5.99 \times 10^{-4}$ , respectively). These enriched KEGG pathways are correlated with myeloid and inflammatory mechanisms. (C) GO enrichment analysis on group 3 identified “extracellular exosome,” “lysosome,” and “plasma membrane” as most significant (Benjamini corrected  $P < 0.05$ ). (D) Expression of myeloid cells from enriched pathways matches *Meox2* expression patterns. (E) Similarly, genes in gliovascular-associated pathways also match *Meox2* expression patterns.

compared to 90% of D2.*Mx*<sup>+/-</sup> females ( $P = 8.02 \times 10^{-6}$  and  $P = 0.199$ , respectively) (Fig. 6C). Therefore, there were significantly more eyes with either moderate or severe axon damage in D2.*Mx*<sup>+/-</sup> mice compared to D2 controls, suggesting that *Meox2* plays a beneficial role in response to OHT in D2 glaucoma.

### *Meox2* Haploinsufficiency Alters Vascular and Myeloid Cell Responses in Aged D2 Mice

To begin to understand mechanism(s) by which *Meox2* haploinsufficiency affects RGC axon damage we first assessed

MEOX2 protein levels in aged mice. Aged D2.*Mx*<sup>+/-</sup> showed on average a 44% reduction in MEOX2 protein levels compared to aged D2 mice (Fig. 7A). Given its predicted role in vascular health and inflammation (Figs. 1–3), we next assessed vasculature in the ONH and retina. There were no overt differences in vascular structures in the ONH of aged D2.*Mx*<sup>+/-</sup> mice compared to aged D2 control mice (Fig. 7B). However, significant differences were observed in the vascular area in the retina. When compared to young controls, an overall decrease in retinal vessel area was observed for both aged D2 and D2.*Mx*<sup>+/-</sup> mice (Figs. 7C, 7D). However, this age-dependent decrease was reduced in retinas from D2.*Mx*<sup>+/-</sup>

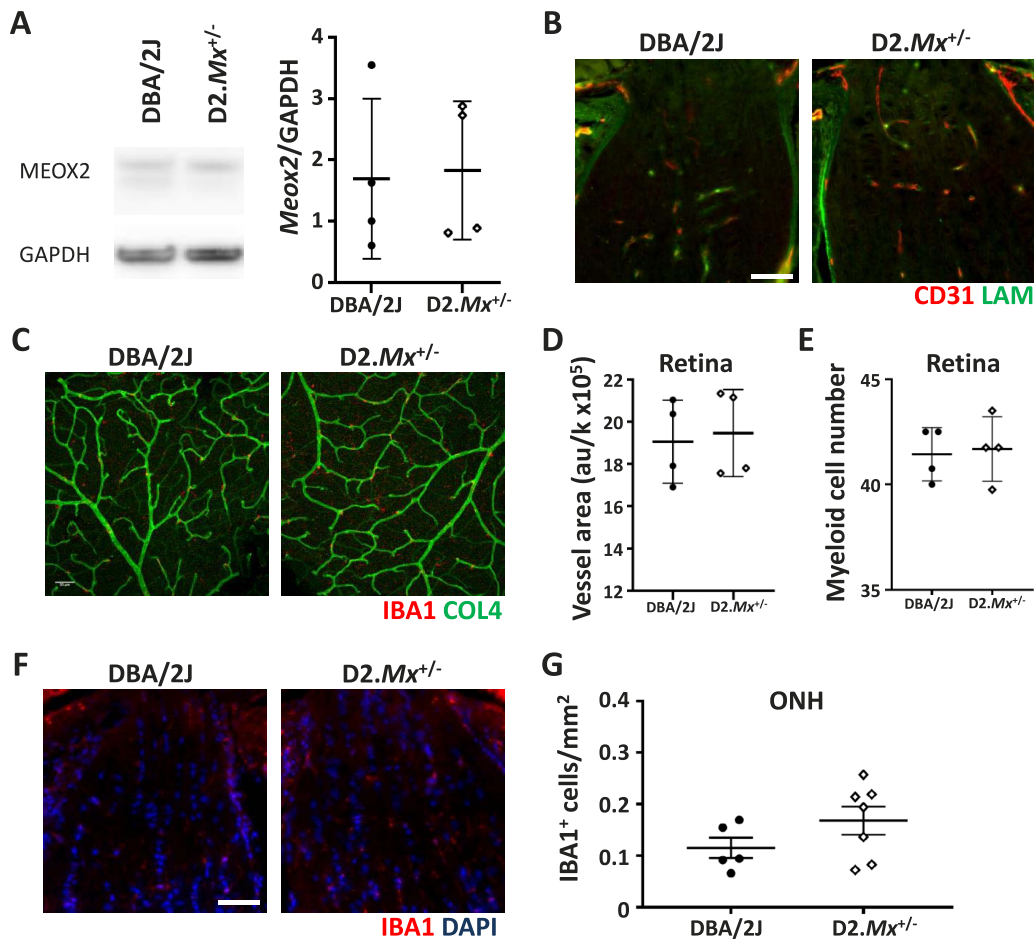


**FIGURE 4.** *Meox2* haploinsufficiency does not cause significant differences in blood vessel area or myeloid cell number in the ONH or retinas of young D2 mice. (A) Western blot analysis on 4 months D2 (DBA/2J) and D2.*Mx*<sup>+/-</sup> retinal tissue probing for MEOX2 protein and GAPDH (glyceraldehyde 3-phosphate dehydrogenase, loading control). There was no significant reduction in MEOX2 between young D2 and D2.*Mx*<sup>+/-</sup> mice ( $P = 0.8847$ ). See Supplementary Figure S3A for full Western blot. (B) Immunofluorescence was performed on 4 months female ONH tissue of both D2 and D2.*Mx*<sup>+/-</sup> labeling for CD31 (endothelial cells) and laminin-111 (LAM, basement membrane). Representative images are shown. There were no observable differences in expression in a sample of  $n = 6$  per group. Scale bar: 50  $\mu\text{m}$ . (C) Immunofluorescence was performed on 4 months female retina tissue of both D2 and D2.*Mx*<sup>+/-</sup> labeling for collagen-4 (COL4, basement membrane) and ionized calcium binding adapter molecule-1 (IBA1, myeloid cells). Representative images are shown. (D) COL4-labeled retinal vessel area was calculated in both 4 months D2 and D2.*Mx*<sup>+/-</sup> mice. There was no significant difference in vessel area in a sample of  $n = 4$  per condition ( $P = 0.7830$ ). (E) IBA1-positive cells were counted in both 4 months D2 and D2.*Mx*<sup>+/-</sup> mice. There was no significant difference in myeloid cell number in a sample of  $n = 4$  per condition ( $P = 0.8097$ ). (F) Immunofluorescence was performed on 4 months female ONH tissue of both D2 and D2.*Mx*<sup>+/-</sup> mice labeling for IBA1 and DAPI. (G) IBA1 and DAPI double-positive cells were quantified as a function of area. There was no significant difference between 4 months D2 and D2.*Mx*<sup>+/-</sup> females ( $P = 0.1782$ ). All  $P$  values were calculated using an unpaired  $t$ -test.

compared to D2 mice. This resulted in significantly greater vessel area in aged D2.*Mx*<sup>+/-</sup> compared to aged D2 mice (Figs. 7C, 7D).

Finally, myeloid cell numbers were assessed. Although there was no difference in myeloid cell numbers between aged D2 and D2.*Mx*<sup>+/-</sup> retinas, there was a significant increase in myeloid cell number between young and aged mice of both genotypes (Fig. 7E). Further, *Meox2* haploinsufficiency significantly affected myeloid cell numbers in the ONH. Specifically, there was a significant increase in myeloid cells in D2 mice from 4 months to 10.5 months. However, there was no significant difference in myeloid cell numbers comparing 8 months to 10.5 months D2 mice. In contrast, for D2.*Mx*<sup>+/-</sup> mice, there was a significant increase in myeloid cells comparing both 4 months to 10.5 months and 8 months to 10.5 months (Figs. 7E, 7G). Therefore, these data support the bioinformatic analyses that *Meox2* plays a role in vascular and myeloid cell changes in the retina and ONH during DBA/2J glaucoma.

## DISCUSSION

Here, we identified *Meox2* as a potential driver of early pathological changes in DBA/2J glaucoma through URA in IPA. A role for *Meox2* in glaucoma has not previously been reported. *Meox2* is an antennapedia-like homeobox-containing transcription factor known to play a variety of important roles during development.<sup>56,57</sup> Mice deficient in *Meox2* (*Mx*<sup>-/-</sup>) are embryonic lethal while *Meox2* haploinsufficient mice are viable. In our previous study, *Meox2* haploinsufficiency exacerbated neurodegenerative phenotypes in a mouse model relevant to Alzheimer's disease.<sup>51</sup> Here, *Meox2* haploinsufficiency increased the number of eyes with moderate and severe axon damage. This, and our previous study, suggest that *Meox2* plays a beneficial role in multiple neurodegenerative diseases. Our primary outcome measure in this study was axon damage. We have previously shown that axon damage assessment correlates closely with a decline in RGC function (by PERG) and changes in axon transport.<sup>15,40-43</sup> However, additional

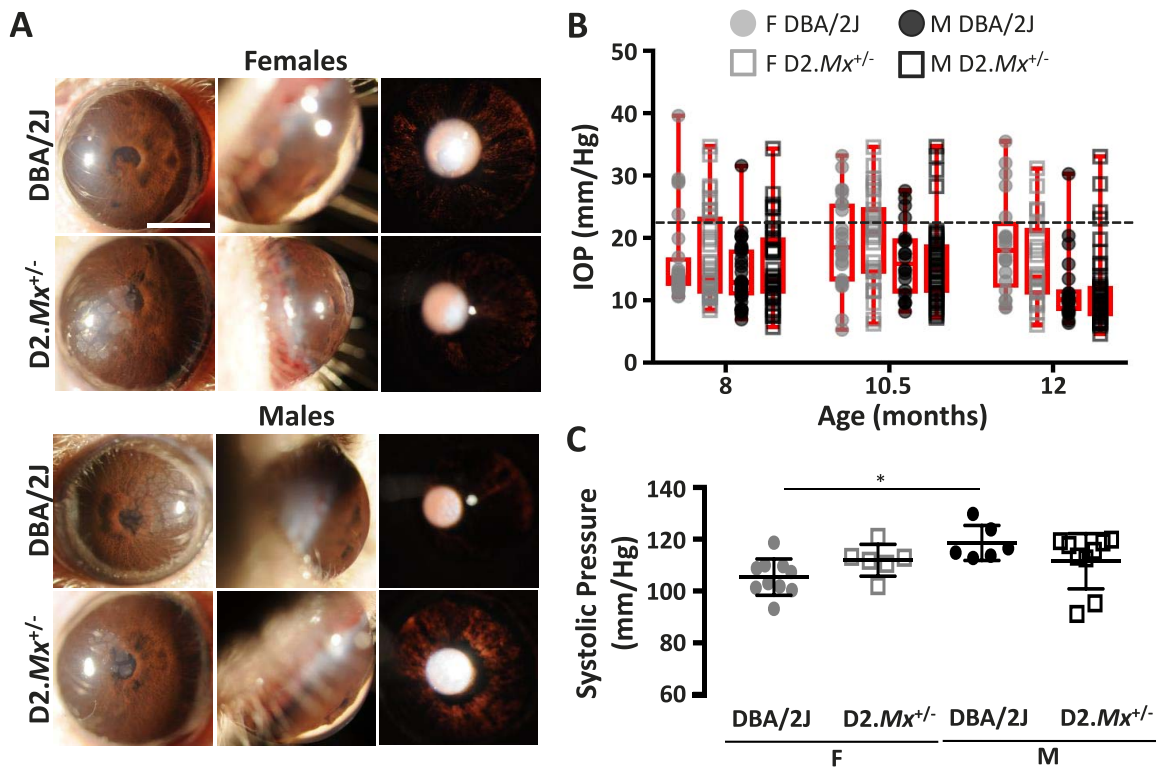


**FIGURE 5.** *Meox2* haploinsufficiency does not affect iris pigment dispersion disease progression or intraocular pressure in DBA/2J mice. (A) Representative slit-lamp images from clinical examinations of 9 months mice. Each row contains three images from the same eye (*left column*, broad beam illumination; *middle column*, relative dimensions of the anterior chamber; *right column*, transillumination). There were no observable differences in iris disease progression from D2 and D2.Mx<sup>+/-</sup> females ( $n = 30, 22$ , respectively) and males ( $n = 16, 18$ , respectively) at 9 months. (B) IOP changes relative to age in D2 and D2.Mx<sup>+/-</sup> mice within sex and age. Dot blots and standard error mean bars were generated using Prism v7.05. Each dot represents the average IOP of a triplicate reading of one eye within one experiment. The dotted line at 21 mm Hg represents a threshold of glaucoma-relevant IOP (8 months: female D2  $n = 27$ , D2.Mx<sup>+/-</sup>  $n = 39$ ; male D2  $n = 33$ , D2.Mx<sup>+/-</sup>  $n = 40$ ) (10.5 months: female D2  $n = 24$ , D2.Mx<sup>+/-</sup>  $n = 30$ ; male D2  $n = 20$ , D2.Mx<sup>+/-</sup>  $n = 46$ ) (12 months: female D2  $n = 20$ , D2.Mx<sup>+/-</sup>  $n = 22$ ; male D2  $n = 22$ , D2.Mx<sup>+/-</sup>  $n = 46$ ). (C) *Meox2* haploinsufficiency did not affect blood pressure when compared to wild-type controls; however, there is a significant difference between DBA/2J females and males at 8 months of age ( $P = 0.0199$ ).

studies are required to determine whether *Meox2* haploinsufficiency has affected the functional state of RGCs. The effect on axon damage was greater in female compared to male mice. IOP elevation is known to occur earlier in female compared to male D2 mice<sup>31</sup> and might therefore be a contributing factor in the greater effect of *Meox2* haploinsufficiency observed in female mice. However, no sex-specific genotype differences were observed in IOP profiles, suggesting that the sex-specific effect on axon damage may be independent of IOP.

The mechanisms by which *Meox2* plays a potential beneficial role in glaucoma are still to be elucidated. Gene networks were identified that are predicted to be targeted by *Meox2*. They were enriched for KEGG pathways associated with cell proliferation, inflammation, extracellular matrix interactions, and NVU-associated pathways. Also, analyses of gene profiling data and k-means analysis predicted KEGG pathways and GO terms relating to vascular responses (e.g., angiogenesis, basement membrane, and extracellular matrix [ECM] maintenance) and neuroinflammation (e.g., myeloid cell responses). We, and others, have shown reduced cerebrovascular density in young *Meox2* haploinsufficient mice.<sup>51,52</sup> Contrary to the observations in the brain, *Meox2* haploinsufficiency did not affect retinal vascular density at a young age. This may be location (brain versus retina) or strain (C57BL/6 vs. DBA/2J) specific. These results provide further evidence of potential differences in neurovascular responses in the retina and brain during disease.

A significant decrease in retinal vascular area between young and aged mice was observed, independent of genotype. However, this age-dependent reduction in vascular area appeared attenuated by *Meox2* haploinsufficiency. Reduced vascular area could be expected to be damaging and therefore maintaining vascular area could be protective. However, *Meox2* haploinsufficiency increased the numbers of eyes with severe optic nerve damage. Multiple factors might contribute to this possible disconnect. The higher density in aged D2.Mx<sup>+/-</sup> compared to DBA/2J mice could be due to retinas from D2.Mx<sup>+/-</sup> mice being at a more advanced stage of disease, correlative with increased axon damage, leading to retinal contraction resulting in increased retinal vascular area. Alternatively, previous studies show that *Meox2* is a regulator of vascular cell proliferation,<sup>58-61</sup> and angiogenesis has been associated with injury response.<sup>62</sup> An increase in vascular proliferation or angiogenesis, on a background of age-dependent decrease in vascular density, could account for the increase in D2.Mx<sup>+/-</sup> compared to DBA/2J mice. These new vessels may not be fully functional. Finally, an increase in basement membrane deposition in D2.Mx<sup>+/-</sup> mice but not in DBA/2J mice would also lead to an increase in vessel area (vessels were visualized using an antibody to collagen 4). This increase in basement membrane deposition may result in reduced function of the retinal vessels, accelerating RGC damage and death.



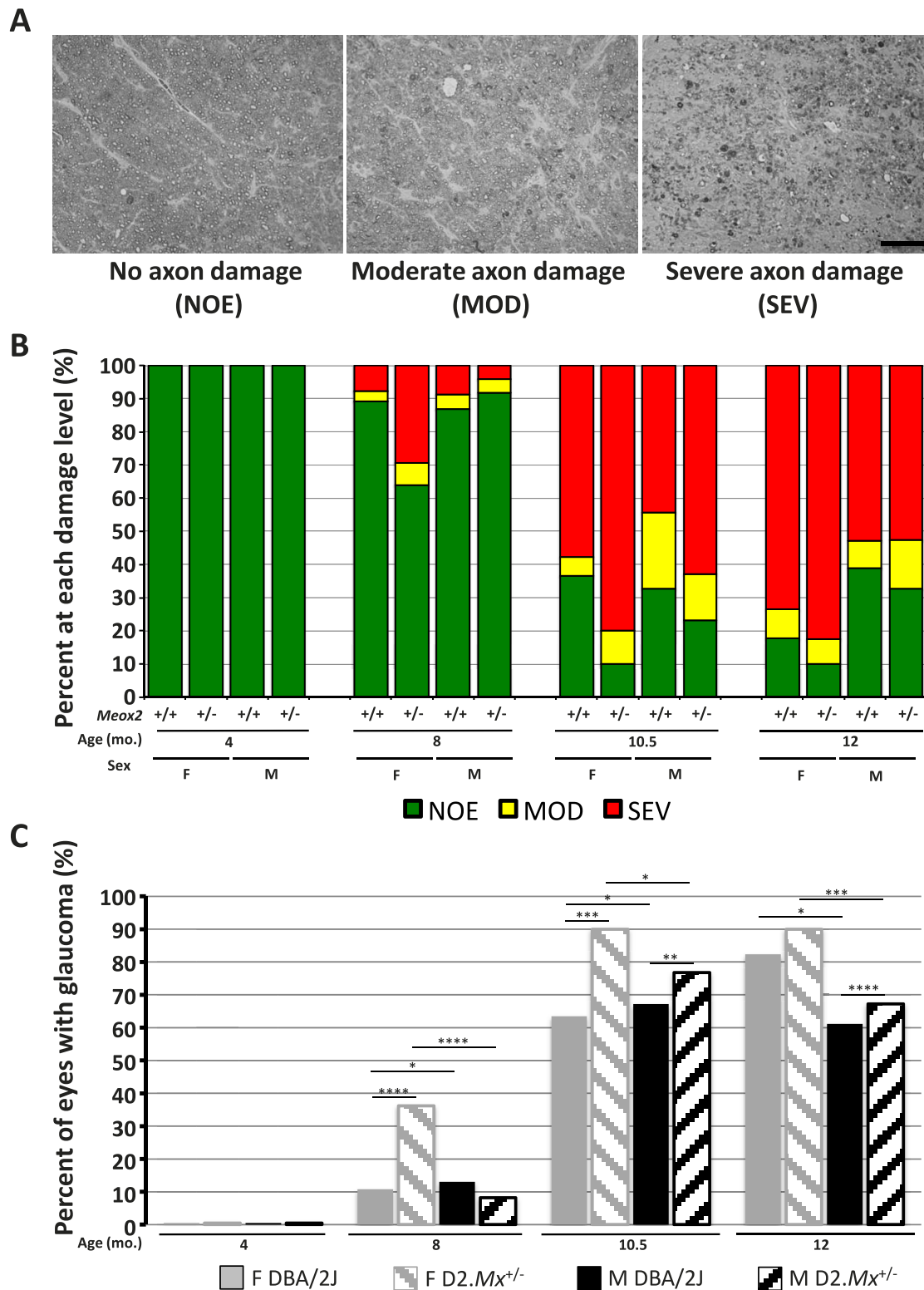


**FIGURE 6.** *Meox2* haploinsufficiency accelerates axon damage in D2 mice. (A) Representative images of DBA/2J optic nerve cross sections stained with paraphenylenediamine (PPD) showing the previously validated morphologic categories of axon damage (NOE, no axonal damage or early molecular changes; MOD, moderate damage; SEV, severe damage). Scale bar: 25  $\mu$ m. (B) Distributions of axon damage of male and female D2 and D2.Mx<sup>+/-</sup> mice aged 4, 8, 10.5, and 12 months. (C) Distributions of optic nerve damage show a significant difference between D2 and D2.Mx<sup>+/-</sup> eyes in females at 8 months ( $\chi^2$  values =  $4.57928 \times 10^{-09}$ , 0.015375192, and  $6.72681 \times 10^{-26}$ , respectively), a significant difference between D2 and D2.Mx<sup>+/-</sup> in females and males at 10.5 months ( $\chi^2$  values = 0.000557957, 0.008348159, 0.01096447, and 0.011528155, respectively), and a significant difference between D2 and D2.Mx<sup>+/-</sup> in females and males at 12 months ( $\chi^2$  values =  $8.02393 \times 10^{-06}$ , 0.039435742, and 0.000221381, respectively). \**P* < 0.05, \*\**P* < 0.01, \*\*\**P* < 0.001, \*\*\*\**P* < 0.0001.



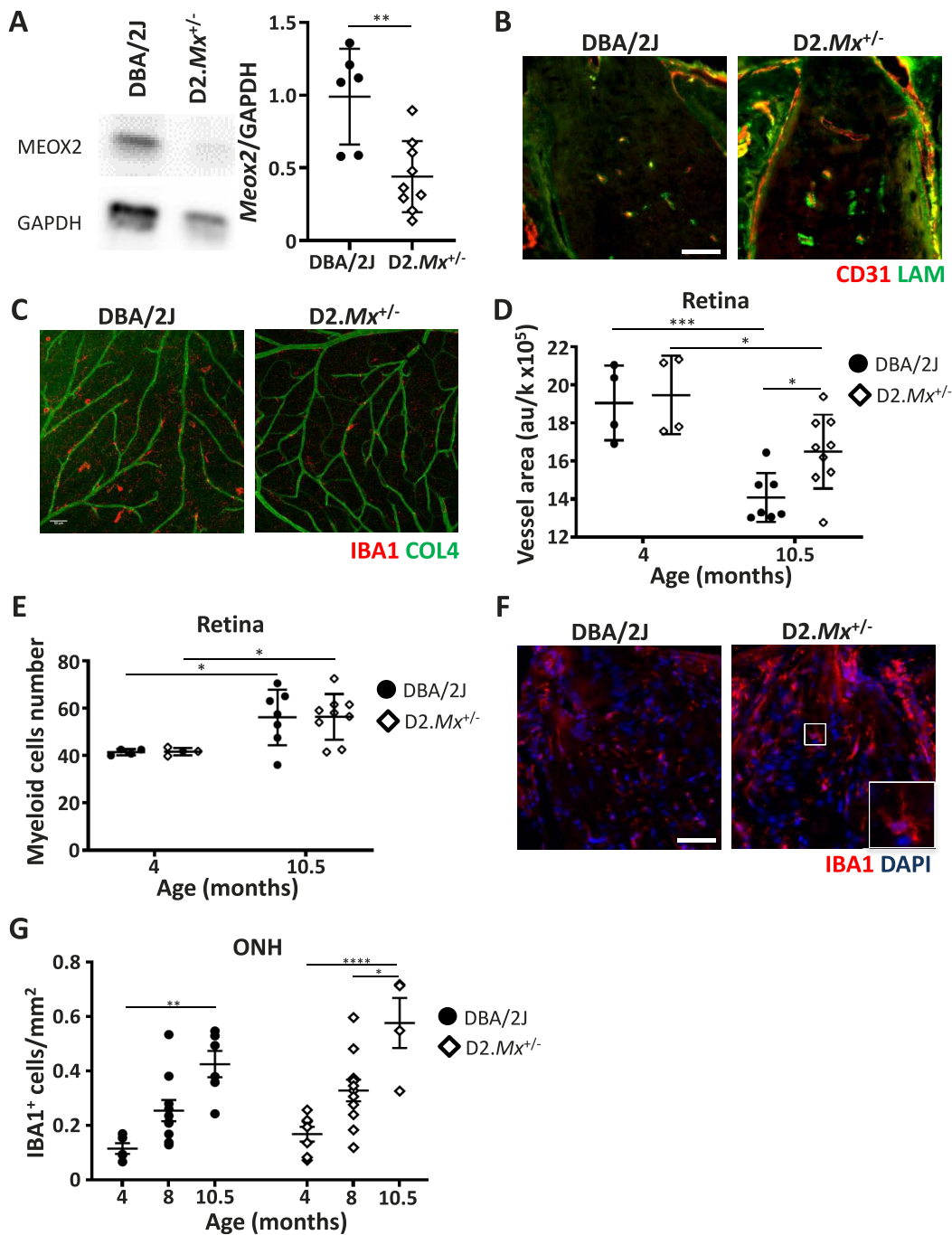


**FIGURE 7.** Aged *Meox2* haploinsufficient mice have reduced vessel density in the retina and increased myeloid cells in the ONH. (A) Western blot analysis on 10.5 months D2 (DBA/2J) and D2.*Mx*<sup>+/-</sup> retinal tissue probing for MEOX2 protein and GAPDH (loading control). There was a 44.4% reduction in MEOX2 protein levels between aged D2 and D2.*Mx*<sup>+/-</sup> mice ( $P = 0.0026$ ). See Figure S3B for full blot. (B) Immunofluorescence was performed on 10.5 months female ONH tissue of both D2 and D2.*Mx*<sup>+/-</sup> labeling for CD31 (endothelial cells) and laminin-111 (LAM, basement membrane). Representative images are shown. There was no observable difference in expression in a sample of  $n = 6$  per condition. Scale bar: 50  $\mu\text{m}$ . (C) Immunofluorescence was performed on 10.5 months female retina tissue of both D2 and D2.*Mx*<sup>+/-</sup> labeling for collagen-4 (COL4, basement membrane) and IBA1 (myeloid cells). Representative images are shown. (D) COL4-labeled retinal vessel area was calculated in both 4 months and 10.5 months D2 and D2.*Mx*<sup>+/-</sup> mice (young data reproduced from Fig. 4D). There was a significant decrease between 4 months and 10.5 months in both D2 and D2.*Mx*<sup>+/-</sup> mice ( $P = 0.0005$  and  $P = 0.0244$ , respectively). However, there was also a significant increase in vessel area between 10.5 months D2.*Mx*<sup>+/-</sup> and D2 mice ( $P = 0.0133$ ). (E) IBA1-positive cells were counted in the retinas of both 4 months and 10.5 months D2 and D2.*Mx*<sup>+/-</sup> mice. There was no significant difference in myeloid cell number in a sample of  $n = 7$  per condition between 10 months D2 and D2.*Mx*<sup>+/-</sup> mice ( $P = 0.9615$ ). However, there was significant increase between 4 months and 10.5 months in both D2 and D2.*Mx*<sup>+/-</sup> mice ( $P = 0.0319$  and  $P = 0.0248$ , respectively). (F) Immunofluorescence was performed on 10.5 months female ONH tissue of both D2 and D2.*Mx*<sup>+/-</sup> mice labeling for IBA1 and DAPI. (G) IBA1 and DAPI double-positive cells were quantified as a function of area. There was no significant difference between 10.5 months D2 and D2.*Mx*<sup>+/-</sup> females ( $P = 0.1782$ ). There is a significant increase in IBA1<sup>+</sup> DAPI<sup>+</sup> cells in D2 and D2.*Mx*<sup>+/-</sup> ONHs from 4 to 10.5 months ( $P = 0.0017$  and  $P < 0.0001$ , respectively). Additionally, there is a significant increase in D2.*Mx*<sup>+/-</sup> ONHs from 8 to 10.5 months ( $P = 0.0148$ ). All  $P$  values were found using a 2-way ANOVA.

Eye diseases such as age-related macular degeneration, choroidal neovascularization, and diabetic retinopathy have been correlated with angiogenesis and vascular regulation by glial cells.<sup>63,64</sup> Neurovascular dysfunction and associated glial responses have also been a topic of much focus in glaucoma.<sup>16,65,66</sup> Interestingly, we recently showed that metabolic stress is a key component of D2 glaucoma.<sup>42</sup> Vascular health is strongly linked to metabolic health, so understanding the interactions between vascular responses and metabolic stress in glaucoma is critical.

In the ONH microarray data, *Meox2* expression increased at the same molecular stage of disease (prior to axon damage) as laminins, collagens, matrix metalloproteinases (MMPs), and tissue inhibitors of MMPs (TIMPs); the cell types secreting these molecules work congruently to maintain NVU function.<sup>67</sup> Quantifying vasculature in the ONH was challenging due to the low density of vasculature in this region and an apparent variability between eyes—even from controls such as the *D2.Gp*<sup>+</sup> mice. Therefore, no observable differences were identified in laminin or CD31 in the ONHs of D2 and *D2.Mx*<sup>+/-</sup> mice. This could be because the antibody used was a pan-laminin that binds primarily LAMA1. The gene expression data show *Lamb2* and *Lamc1* being upregulated. Therefore, immunoassays for specific laminin monomers and collagens could be more informative of NVU changes in the ONH in glaucoma, particularly considering the observation that retinal vasculature is altered. In support of a role of ONH vascular in glaucoma, a recent study by Zhu and colleagues<sup>68</sup> used C57BL/6 mice to show that blood vessels in the ONH thicken with age and after induction of high IOP in young mice. This type of analysis is more challenging to perform in D2 mice given the variable age of onset of IOP elevation.

The question of beneficial versus damaging immune responses has led to predictions of early inflammatory signaling being protective to RGCs following axon injury and prolonged IOP elevation evolving into a chronic and damaging inflammation.<sup>13,69-71</sup> Specific immune-like functions have been found to be both protective and damaging in glaucoma.<sup>15,72-74</sup> Disruption of the endothelin system and complement component *C1qa* reduced the numbers of eyes with axon damage in D2 mice, suggesting they play a damaging role.<sup>14</sup> In contrast, knocking out complement component C3 increased the numbers of eyes with glaucoma, suggesting it plays a beneficial role.<sup>15</sup> Like C3, *Meox2* appears to exert a beneficial response mediated at least in part through immune responses—in this case in myeloid cells. Interestingly, a recent paper showed that knocking down C3 in RGCs using a viral approach appeared to protect from RGC loss, suggesting an additional layer of complexity whereby cell type-specific responses of the same gene/pathways may have opposing effects at different stages in glaucoma.<sup>74</sup>

In addition to changes in the vascular area, *Meox2* appears to also impact myeloid cell numbers. In this study we refer to myeloid cell responses, not microglial responses, as monocytes/macrophage-like cells infiltrate from the periphery during early stages in DBA/2J glaucoma.<sup>32,43</sup> Anti-IBA1, the antibody used to label myeloid cells, does not distinguish resident microglia from infiltrating monocytes/macrophages. The role of these different myeloid cell subtypes in glaucoma is not clear. Microglia activation in response to elevated IOP has been seen in many studies, and early microglia changes, such as microgliosis prior to IOP damage, has been reported to correlate with late severity of nerve pathology.<sup>75,76</sup> Therefore, in combination, these studies chronicle a close relation between elevated IOP and microglial activation. A similarly complex relationship between disease insult and microglia activation is being reported for other neurodegenerative diseases.<sup>77</sup> For instance, in Alzheimer's Disease, microglia

may execute a beneficial response to clear amyloid<sup>78</sup> but also aberrantly prune synapses.<sup>79</sup> Multiple studies are now using single-cell profiling approaches to define subtypes of microglia and other myeloid cells (monocytes/macrophages) to develop strategies to target damaging but not beneficial cells.<sup>80</sup> Similar approaches should be employed for glaucoma. Understanding the relationship between vascular health and myeloid responses will also be important to better inform potential strategies for treatments for glaucoma.

D2 mice develop glaucoma due to mutations in *Gpnmb* and *Tyrp1* that cause the iris disease that is necessary for IOP elevation.<sup>29,30</sup> This is evident in the *D2.Gp*<sup>+</sup> strain that develops neither high IOP nor RGC loss. This allowed us to assess *Meox2* function in the absence of IOP elevation. *Meox2* haploinsufficiency did not cause iris disease, increased IOP, or axonal damage in *D2.Gp*<sup>+</sup> mice (Supplementary Fig. S1). Myeloid cell numbers did not change in *D2.Gp*<sup>+</sup> or *D2.Gp*<sup>+</sup>*Mx*<sup>+/-</sup> mice between 4 months and 10.5 months. However, there are fewer myeloid cells when comparing 10.5 months *D2.Gp*<sup>+</sup> and *D2.Gp*<sup>+</sup>*Mx*<sup>+/-</sup> mice (Supplementary Fig. S2). This suggests that *Meox2* may play a role in myeloid cell health, maintenance, or turnover during aging. For instance, there may be an increase in the rate of myeloid cell turnover in *D2.Gp*<sup>+</sup>*Mx*<sup>+/-</sup> compared to *D2.Gp*<sup>+</sup> mice. In this study, we assessed mice up to only 12 months—considered midlife in humans. Additional analyses of older mice would be required to fully determine whether *Meox2* plays a key role in myeloid cell maintenance and turnover.

In summary, we have identified *Meox2* as a potential regulator of early, beneficial stages of glaucoma in DBA/2J mice. We predict that its effect is mediated in part through modified vascular and myeloid cell responses. This work provides further evidence that the earliest changes in response to IOP elevation are beneficial and that enhancing these responses may delay onset of visual defects in human glaucomas.

### Acknowledgments

The authors thank Amy Bell and Mimi deVries for IOP measurements, Jeffrey Harder for training in clinical assessments, and Jennifer Ryan and In Vivo Physiology at The Jackson Laboratory for performing blood pressure measurements. They also thank Richard Libby for intellectual insights.

Supported by EY027701 (GRH) and EY011721 (SWMJ). Simon John is an investigator of the Howard Hughes Medical Institute. Gareth Howell is the Diana Davis Foundation Chair for Glaucoma Research at The Jackson Laboratory.

Disclosure: **R.A. Buchanan**, None; **K.E. Foley**, None; **K.W. Pepper**, None; **A.M. Reagan**, None; **K.J. Keezer**, None; **A.A. Hewes**, None; **C.A. Diemler**, None; **C. Preuss**, None; **I. Soto**, None; **S.W.M. John**, None; **G.R. Howell**, None

### References

- Burgoyne CF. A biomechanical paradigm for axonal insult within the optic nerve head in aging and glaucoma. *Exp Eye Res.* 2010;93:120-132.
- Nickells RW, Howell GR, Soto I, John SWM. Under pressure: cellular and molecular responses during glaucoma, a common neurodegeneration with axonopathy. *Annu Rev Neurosci.* 2012;35:153-179.
- Downs JC, Roberts MD, Burgoyne CF. Mechanical environment of the optic nerve head in glaucoma. *Optom Vis Sci.* 2008;85:425-435.
- Fechter RD, Weinreb RN. Mechanisms of optic nerve damage in primary open angle glaucoma. *Surv Ophthalmol.* 1994;39:23-42.

5. Anderson DR, Hendrickson A. Effect of intraocular pressure on rapid axoplasmic transport in monkey optic nerve. *Invest Ophthalmol.* 1974;13:771-783.
6. Quigley H, Anderson DR. The dynamics and location of axonal transport blockade by acute intraocular pressure elevation in primate optic nerve. *Invest Ophthalmol.* 1976; 15:606-616.
7. Quigley HA, Addicks EM. Regional differences in the structure of the lamina cribrosa and their relation to glaucomatous optic nerve damage. *Arch Ophthalmol.* 1981;99:137-143.
8. Quigley HA, Addicks EM, Green WR, Maumenee AE. Optic nerve damage in human glaucoma. II. The site of injury and susceptibility to damage. *Arch Ophthalmol.* 1981;99:635-649.
9. Quigley HA, Green RW. The histology of human glaucoma cupping and optic nerve damage: clinicopathologic correlation in 21 eyes. *Ophthalmology.* 1979;86:1803-1827.
10. Fukuchi T, Sawaguchi S, Hara H, Shirakashi M, Iwata K. Extracellular matrix changes of the optic nerve lamina cribrosa in monkey eyes with experimentally chronic glaucoma. *Graefes Arch Clin Exp Ophthalmol.* 1992;30:421-427.
11. Hernandez MR, Luo XX, Andrzejewska W, Neufeld AH. Age-related changes in the extracellular matrix of the human optic nerve head. *Am J Ophthalmol.* 1989;107:476-484.
12. Hernandez MR, Ye H. Glaucoma: changes in extracellular matrix in the optic nerve head. *Ann Med.* 1993;25:309-315.
13. Bosco A, Steele MR, Vetter ML. Early microglia activation in a mouse model of chronic glaucoma. *J Comp Neurol.* 2011;519: 599-620.
14. Howell GR, MacNicol KH, Braine CE, et al. Combinatorial targeting of early pathways profoundly inhibits neurodegeneration in a mouse model of glaucoma. *Neurobiol Dis.* 2014; 71:44-52.
15. Harder JM, Braine CE, Williams PA, et al. Early immune responses are independent of RGC dysfunction in glaucoma with complement component C3 being protective. *Proc Natl Acad Sci U S A.* 2017;114:E3839-E3848.
16. Soto I, Howell GR. The complex role of neuroinflammation in glaucoma. *Cold Spring Harb Perspect Med.* 2014;4:a017269.
17. Cueva Vargas JL, Di Polo A. Neuroinflammation in glaucoma: soluble tumor necrosis factor alpha and the connection with excitotoxic damage. *Neural Regen Res.* 2016;11:424-426.
18. Prada D, Harris A, Guidoboni G, Siesky B, Huang AM, Arciero J. Autoregulation and neurovascular coupling in the optic nerve head. *Surv Ophthalmol.* 2016;61:164-186.
19. Zlokovic BV. Neurodegeneration and the neurovascular unit. *Nat Med.* 2010;16:1370-1371.
20. Zlokovic BV. Neurovascular pathways to neurodegeneration in Alzheimer's disease and other disorders. *Nat Rev Neurosci.* 2011;12:723-738.
21. Ahmed F, Brown KM, Stephan DA, Morrison JC, Johnson EC, Tomarev SI. Microarray analysis of changes in mRNA levels in the rat retina after experimental elevation of intraocular pressure. *Invest Ophthalmol Vis Sci.* 2004;45:1247-1258.
22. Johnson EC, Jia L, Cepurna WO, Doser TA, Morrison JC. Global changes in optic nerve head gene expression after exposure to elevated intraocular pressure in a rat glaucoma model. *Invest Ophthalmol Vis Sci.* 2007;48:3161-3177.
23. Steele MR, Inman DM, Calkins DJ, Horner PJ, Vetter ML. Microarray analysis of retinal gene expression in the DBA/2J model of glaucoma. *Invest Ophthalmol Vis Sci.* 2006;47:977-985.
24. Yang Z, Quigley HA, Pease ME, et al. Changes in gene expression in experimental glaucoma and optic nerve transection: the equilibrium between protective and detrimental mechanisms. *Invest Ophthalmol Vis Sci.* 2007;48: 5539-5548.
25. Panagis L, Zhao X, Ge Y, Ren L, Mittag TW, Danias J. Gene expression changes in areas of focal loss of retinal ganglion cells in the retina of DBA/2J mice. *Invest Ophthalmol Vis Sci.* 2010;51:2024-2034.
26. Panagis L, Zhao X, Ge Y, Ren L, Mittag TW, Danias J. Retinal gene expression changes related to IOP exposure and axonal loss in DBA/2J mice. *Invest Ophthalmol Vis Sci.* 2011;52: 7807-7816.
27. Howell GR, Macalinao DG, Sousa GL, et al. Molecular clustering identifies complement and endothelin induction as early events in a mouse model of glaucoma. *J Clin Invest.* 2011;121:1429-1444.
28. Howell GR, Walton DO, King BL, Libby RT, John SW. Datgan, a reusable software system for facile interrogation and visualization of complex transcription profiling data. *BMC Genomics.* 2011;12:429.
29. Chang B, Smith RS, Hawes NL, et al. Interacting loci cause severe iris atrophy and glaucoma in DBA/2J mice. *Nat Genet.* 1999;21:405-409.
30. Anderson MG, Smith RS, Hawes NL, et al. Mutations in genes encoding melanosomal proteins cause pigmentary glaucoma in DBA/2J mice. *Nat Genet.* 2002;30:81-85.
31. Libby RT, Anderson MG, Pang IH, et al. Inherited glaucoma in DBA/2J mice: pertinent disease features for studying the neurodegeneration. *Vis Neurosci.* 2005;22:637-648.
32. Howell GR, Soto I, Zhu X, et al. Radiation treatment inhibits monocyte entry into the optic nerve head and prevents neuronal damage in a mouse model of glaucoma. *J Clin Invest.* 2012;122:1246-1261.
33. Huang DW, Sherman BT, Lempicki RA. Systematic and integrative analysis of large gene lists using DAVID bioinformatics resources. *Nat Protoc.* 2009;4:44-57.
34. John SW, Hagaman JR, MacTaggart TE, Peng L, Smithes O. Intraocular pressure in inbred mouse strains. *Invest Ophthalmol Vis Sci.* 1997;38:249-253.
35. Savinova OV, Sugiyama F, Martin JE, et al. Intraocular pressure in genetically distinct mice: an update and strain survey. *BMC Genet.* 2001;2:12.
36. Sugiyama F, Churchill GA, Li R, et al. QTL associated with blood pressure, heart rate, and heart weight in CBA/CaJ and BALB/cJ mice. *Physiol Genomics.* 2002;10:5-12.
37. Anderson MG, Libby RT, Gould DB, Smith RS, John SW. High-dose radiation with bone marrow transfer prevents neurodegeneration in an inherited glaucoma. *Proc Natl Acad Sci U S A.* 2005;102:4566-4571.
38. Libby RT, Li Y, Savinova OV, et al. Susceptibility to neurodegeneration in a glaucoma is modified by Bax gene dosage. *PLoS Genet.* 2005;1:17-26.
39. Anderson MG, Libby RT, Mao M, et al. Genetic context determines susceptibility to intraocular pressure elevation in a mouse pigmentary glaucoma. *BMC Biol.* 2006;4:20.
40. Howell GR, Libby RT, Jakobs TC, et al. Axons of retinal ganglion cells are insulted in the optic nerve early in DBA/2J glaucoma. *J Cell Biol.* 2007;179:1523-1537.
41. Howell GR, Libby RT, Marchant JK, et al. Absence of glaucoma in DBA/2J mice homozygous for wild-type versions of GpnmB and Tyrp1. *BMC Genet.* 2007;8:45.
42. Williams PA, Harder JM, Foxworth NE, et al. Vitamin B3 modulates mitochondrial vulnerability and prevents glaucoma in aged mice. *Science.* 2017;355:756-760.
43. Williams PA, Braine CE, Kizhatil K, et al. Inhibition of monocyte-like cell extravasation protects from neurodegeneration in DBA/2J glaucoma. *Mol Neurodegener.* 2019;14:6.
44. Reagan AM, Gu X, Paudel S, et al. Age-related focal loss of contractile vascular smooth muscle cells in retinal arterioles is



- accelerated by caveolin-1 deficiency. *Neurobiol Aging*. 2018; 71:1-12.
45. Zudaire E, Gambardella L, Kurcz C, Vermeren S. A computational tool for quantitative analysis of vascular networks. *PLoS One*. 2011;6:e27385.
  46. Huang W, Fileta JB, Dobberfuhr A, et al. Calcineurin cleavage is triggered by elevated intraocular pressure, and calcineurin inhibition blocks retinal ganglion cell death in experimental glaucoma. *Proc Natl Acad Sci U S A*. 2005;102:12242-12247.
  47. Irnaten M, Zhdanov A, Brennan D, et al. Activation of the NFAT-calcium signaling pathway in human lamina cribrosa cells in glaucoma. *Invest Ophthalmol Vis Sci*. 2018;59:831-842.
  48. Qu J, Wang D, Grosskreutz CL. Mechanisms of retinal ganglion cell injury and defense in glaucoma. *Exp Eye Res*. 2010;91:48-53.
  49. Qu J, Matsouaka R, Betensky RA, Hyman BT, Grosskreutz CL. Calcineurin activation causes retinal ganglion cell degeneration. *Mol Vis*. 2012;18:2828-2838.
  50. Faralli JA, Clark RW, Filla MS, Peters DM. NFATc1 activity regulates the expression of myocilin induced by dexamethasone. *Exp Eye Res*. 2015;130:9-16.
  51. Soto I, Grabowska WA, Onos KD, et al. Meox2 haploinsufficiency increases neuronal cell loss in a mouse model of Alzheimer's disease. *Neurobiol Aging*. 2016;42:50-60.
  52. Wu Z, Guo H, Chow N, et al. Role of the MEOX2 homeobox gene in neurovascular dysfunction in Alzheimer disease. *Nat Med*. 2005;11:959-965.
  53. Klein BEK, Klein R, Knudtson MD. Intraocular pressure and systemic blood pressure: longitudinal perspective: the Beaver Dam Eye Study. *Br J Ophthalmol*. 2005;89:284-287.
  54. Caprioli J, Coleman AL; Blood Flow in Glaucoma Discussion. blood pressure, perfusion pressure, and glaucoma. *Am J Ophthalmol*. 2010;149:704-712.
  55. Cantor E, Méndez F, Rivera C, Castillo A, Martínez-Blanco A. Blood pressure, ocular perfusion pressure and open-angle glaucoma in patients with systemic hypertension. *Clin Ophthalmol*. 2018;12:1511-1517.
  56. Mankoo BS, Collins NS, Ashby P, et al. Mox2 is a component of the genetic hierarchy controlling limb muscle development. *Nature*. 1999;400:69-73.
  57. Mankoo BS, Skuntz S, Harrigan I, et al. The concerted action of Meox homeobox genes is required upstream of genetic pathways essential for the formation, patterning and differentiation of somites. *Development*. 2003;130:4655-4664.
  58. Gorski DH, Leal AD. Inhibition of endothelial cell activation by the homeobox gene Gax. *J Surg Res*. 2003;111:91-99.
  59. Smith RC, Branellec D, Gorski DH, et al. p21CIP1-mediated inhibition of cell proliferation by overexpression of the gax homeodomain gene. *Genes Dev*. 1997;11:1674-1689.
  60. Witzenbichler B, Kureishi Y, Luo Z, Le Roux A, Branellec D, Walsh K. Regulation of smooth muscle cell migration and integrin expression by the Gax transcription factor. *J Clin Invest*. 1999;104:1469-1480.
  61. Chen Y, Rabson AB, Gorski DH. MEOX2 regulates nuclear factor-B activity in vascular endothelial cells through interactions with p65 and IB. *Cardiovasc Res*. 2010;87:723-731.
  62. Yang Y, Kimura-Ohba S, Thompson JE, et al. Vascular tight junction disruption and angiogenesis in spontaneously hypertensive rat with neuroinflammatory white matter injury. *Neurobiol Dis*. 2018;114:95-110.
  63. Ambati J, Fowler BJ. Mechanisms of age-related macular degeneration. *Neuron*. 2013;75:26-39.
  64. Capitao M, Soares R. Angiogenesis and inflammation crosstalk in diabetic retinopathy. *J Cell Biochem*. 2016;117:2443-2453.
  65. Cai W, Zhang K, Li P, et al. Dysfunction of the neurovascular unit in ischemic stroke and neurodegenerative diseases: an aging effect. *Ageing Res Rev*. 2017;34:77-87.
  66. Nikells RW, Howell GR, Soto I, John SW. Under pressure: cellular and molecular responses during glaucoma, a common neurodegeneration with axonopathy. *Annu Rev Neurosci*. 2012;35:153-179.
  67. Muoio V, Persson PB, Sandeski MM. The neurovascular unit - concept review. *Acta Physiol*. 2014;210:790-798.
  68. Zhu Y, Pappas AC, Wang R, Seifert P, Sun D, Jakobs TC. Ultrastructural morphology of the optic nerve head in aged and glaucomatous mice. *Invest Ophthalmol Vis Sci*. 2018;59:3984-3996.
  69. Neufeld AH. Microglia in the optic nerve head and the region of parapapillary chorioretinal atrophy in glaucoma. *Arch Ophthalmol*. 1999;117:1050-1056.
  70. Hanisch UK, Kettenmann H. Microglia: active sensor and versatile effector cells in the normal and pathologic brain. *Nat Neurosci*. 2007;10:1387-1394.
  71. Wei X, Cho KS, Thee EF, Jager MJ, Chen DF. Neuroinflammation and microglia in glaucoma: time for a paradigm shift. *J Neurosci Res*. 2019;97:70-76.
  72. Howell GR, Soto I, Libby RT, John SW. Intrinsic axonal degeneration pathways are critical for glaucomatous damage. *Exp Neurol*. 2013;26:54-61.
  73. Howell GR, Soto I, Ryan M, Graham LC, Smith RS, John SW. Deficiency of complement component 5 ameliorates glaucoma in DBA/2J mice. *J Neuroinflammation*. 2013;10:76.
  74. Bosco A, Anderson SR, Breen KT, et al. Complement C3-targeted gene therapy restricts onset and progression of neurodegeneration in chronic mouse glaucoma. *Mol Ther*. 2018;26:2379-2396.
  75. Bosco A, Romero CO, Breen KT, et al. Neurodegeneration severity can be predicted from early microglia alterations monitored in vivo in a mouse model of chronic glaucoma. *Dis Model Mech*. 2015;8:443-455.
  76. Bosco A, Breen KT, Anderson SR, Steele MR, Calkins DJ, Vetter ML. Glial coverage in the optic nerve expands in proportion to optic axon loss in chronic mouse glaucoma. *Exp Eye Res*. 2016;150:34-43.
  77. Kipnis J, Filiano AJ. The central nervous system: privileged by immune connections. *Nat Rev Immunol*. 2018;18:83-84.
  78. Ries M, Sastre M. Mechanisms of A $\beta$  clearance and degradation by glial cells. *Front Aging Neurosci*. 2016;8:160.
  79. Hong S, Beja-Glasser VE, Nfonoyim BM, et al. Complement and microglia mediate early synapse loss in Alzheimer mouse models. *Science*. 2016;352:712-716.
  80. Keren-Shaul H, Spinrad A, Weiner A, et al. A unique microglia type associated with restricting development of Alzheimer's disease. *Cell*. 2017;169:1276-1290.